HIGH TORQUE LOW INRUSH CURRENT MOTOR DESIGN OR VOLTAGE RECOVERY DEPENDANCE FOR LOADED START CONDITIONS

Paper No. PCIC- 2022 xxxx

Dr. Frederemar Rüncos, Prof. Eng
WEG
Jaraguá do Sul
Brazil
fredemar@weg.net

Michael Bachmeyer, Eng
WEG
Jaraguá do Sul
Brazil
mbachmeyer@weg.net

Miguel Sarris, P.E, Eng
DORIS INC
Houston
USA
msarris@doris-inc.com

Adrain Stafford, Eng
MODEC
Houston
USA
Adrain.Stafford@modec.com

Abstract – With today's increased focus on net-zero emissions, Oil & Gas companies around the world are working towards reducing flaring as much as possible to reduce the environmental impact.

Topsides footprint and real estate inside electrical buildings is a luxury for new and existing facilities, so gear boxes, Adjustable Speed Drives (ASD), and other methods to reduce starting currents, are less desirable options. In the Industry there is a common misconception around low inrush current motors, regarding weight, kW and footprint increments, when compared with a typical direct on-line (DOL) induction motor with the same parameters (kW);

This misconception assumes that the only benefit is the low inrush, but torque is jeopardized for low inrush motors. In this paper we will present the benefits of low inrush motors, and how higher torques can be achieved to clarify this misconception.

Index Terms – induction motor, low inrush current, starting duty.

I. INTRODUCTION

For large centrifugal gas compressors located on a Floating Production Unit (FPU), for example, a gas blowdown to facilitate the electric motor unloaded starting condition may no longer be permitted. This can force a loaded start requirement of the compressor, the typical low inrush current motor solution may not be a good technical fit because of the low torque the motor develops at reduced voltage. Therefore, the low inrush current motors must be redesigned to meet these new requirements.

This paper will propose solution possibilities based on the new characteristics of the driven equipment load but keeping the level of impact on the power supply low. For this purpose, a special design of motors with low inrush current, but with higher torque, will be proposed. This solution will be compared to the today's approach of using standard low inrush current motor, solutions that relies only on voltage recovery from the generator's Alternator Voltage Regulator (AVR) during motor acceleration.

A test case will be presented where a high torque low inrush current 18 MW induction motor driving a gas compressor with loaded start condition is started DOL with 80% reduced voltage. This solution will be compared with a traditional low inrush current equivalent motor but relying on the generator AVR voltage recovery.

Large gas centrifugal compressors normally have a suction throttle valve to regulate the suction pressure down to design pressure, that is, minimum pressure. The drop of suction pressure is a waste of energy but with this device the load torque curve in the starting process is reduced. Thus, the driven load can be classified as Light Start Duty (LSD) and the typical Low Inrush Current (LIC) motor is a very effective solution [2].

For the dynamic analysis purposes, an industrial load can be classified as a LSD when low inertia is present, low starting torque and low load torque during acceleration process. These characteristics can be summarized as:

$$\text{Light Start Duty [LSD]}\begin{cases} J_{\text{Load}} < 1.0 \times J_{\text{Motor}} \\ T_{\text{Starting}} < 0.30 \ (\text{pu}) \\ T_{\text{EndAccelaration}} < 0.60 \ (\text{pu}) \end{cases} \quad (1)$$

In inequalities (1) are:

J_{Motor} Motor inertia in kgm²

J_{Load} Load inertia in kgm²

T_{Starting} Load starting torque in (pu)

$T_{\text{EndAcceleration}}$ Load torque in end of acceleration in (pu)

All parameters of inequalities (1) are referred to motor shaft. When the motors are required to accelerate the compressors at full pressure, without the aid of the throttle valve, we can classify the load as Normal Start Duty (NSD). This results in a greater thermal stress for the motor and presents a greater degree of difficulty in the design.

For the dynamic analysis purposes, an industrial load can be classified as a NSD when normal inertia is present, normal starting torque and normal torque during the acceleration process. Therefore, the NSD meets the following load characteristics:

$$\text{Normal Start Duty [NSD]}\begin{cases} J_{\text{Load}} < 3.0 \times J_{\text{Motor}} \\ T_{\text{Starting}} < 0.50 \ (\text{pu}) \\ T_{\text{EndAcceleration}} < 1.00 \ (\text{pu}) \end{cases} \quad (2)$$

In inequalities (2) are:

J_{Motor} Motor inertia in kgm²

J_{Load} Load inertia in kgm²

T_{Starting} Load starting torque in (pu)

$T_{\text{EndAcceleration}}$ Load torque in end of acceleration in (pu)

All parameters of inequalities (2) are referred to motor shaft.

The typical LIC motor solution may not be a good technical solution because of the low torque the motor develops at reduced voltage. Therefore, the typical LIC motor needs to be redesigned to meet NSD requirements.

Industrial loads that have large inertia and high starting torque dynamically can be classified as Heavy Starting Duty (HSD).

The HSD category has the following characteristics:

$$\text{Heavy Start Duty [HSD]}\begin{cases} J_{\text{Load}} \geq 3.0 \times J_{\text{Motor}} \\ T_{\text{Starting}} \geq 0.50 \ (\text{pu}) \\ T_{\text{EndAcceleration}} \geq 1.00 \ (\text{pu}) \end{cases} \quad (3)$$

In inequalities (3) are:

J_{Motor} Motor inertia in kgm²

J_{Load} Load inertia in kgm²

T_{Starting} Load starting torque in (pu)

$T_{\text{EndAcceleration}}$ Load torque in end of acceleration in (pu)

All parameters of inequalities (3) are referred to motor shaft.

The case to be analyzed in this paper is related to loads classified as LSD and NSD, and therefore, loads classified as HSD will not be considered.

Fig.1 illustrates the concept of LSD and NSD typical loads torque curves.

The redesign of the LIC motor to meet this new requirement will require a great effort, based on knowledge and experience with motor's design and manufacturing, with special focus on alloys of conductive materials for the construction of the new squirrel cage rotor.

This paper will propose possible solutions based on the new characteristics of the driven equipment load but keeping low the impact on the power supply or consumption.

The first solution is today's conventional approach of using the typical LIC motor, with generator voltage recovery through the AVR during motor acceleration.

The second solution is a special design of motors with low inrush current, but with higher torque, to guarantee the acceleration process without dependency of voltage recovery.

II. LOW INRUSH CURRENT MOTOR (LIC) WITH VOLTAGE RECOVERY

For our study we will consider a real case of a centrifugal compressor with the following data, shown in Table I. The starting torque and the torque at the end of the acceleration process are in per-unit (pu).

Considering the torque required at the beginning and at the end of acceleration, this compressor features a high torque curve that is classified as NSD. Fig. 1 shows the torque curve of the compressor which at the beginning is within the LSD region, but at the end of acceleration period is within the area of the NSD load. This characteristic of the torque curve makes the typical LIC motor difficult to accelerate the load to the nominal speed when starting at 80% of the rated voltage.

TABLE I
LOAD NOMINAL DATA

Driven Machine	Centrifugal Compressor	Units
Load Torque Curve	Parabolic	
Nominal speed	1785	rpm
Nominal torque	81,850.0	Nm
Starting torque	0.04	pu
Torque at the end of acceleration	0.85	pu
Load Inertia	1,310.0	kgm2

The compressor torque curve at the end of acceleration period is higher because the compressor, due to environmental requirements or restrictions, cannot use a throttle valve during the start-up process.

In general, when the motor starts direct on-line (DOL) with a starting current between 3.0 pu and 4.0 pu, it is considered a LIC motor. Typical LIC motor the inrush current is close to 3.0 pu.

When the load classified as NSD has starting torque closer to the upper limit 0.50 pu, the higher torque LIC motor design becomes more complex and the starting current in this case approaches 4.0 pu.

Squirrel Cage heating during the starting process also becomes a problem that needs to be minimized in the motor design.

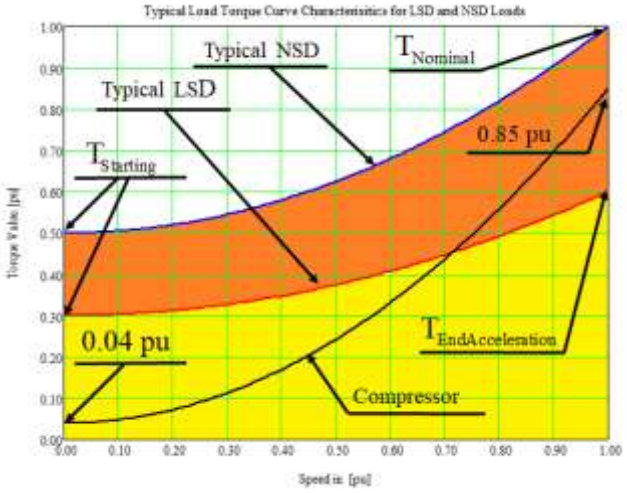

Fig.1 Compressor and load torque curves.

Typical loads classified as NSD have a very low starting torque and the torque at the end of the acceleration higher, according to the example shown in Fig. 1. This more significant increase in torque as a function of speed requires a more elaborated starting condition. This discussion about the process of accelerating this type of load, that is, NSD load, is the main objective of the paper.

Let's begin the study of the driver selection of this compressor with a typical LIC motor with the following nominal data according Table II.

TABLE II

LIC MOTOR NOMINAL DATA

Item	Value	units
Output	18,000.0	kW
Voltage	13.8	kV
Frequency	60	Hz
Nominal speed	1,775.6	rpm
Temperature rise	80	K
Protection degree	IP56	
Cooling system	IC81W	
Hazardous area	Zone 1 – Ex(p)	

The motor's specification requires that the sum of all applied margins is 15% of the highest operating power. This motor is designed for the following performance data shown in Table III.

TABLE III

LIC MOTOR DESIGN DATA

Item	Value	units
Nominal torque	96,000.0	Nm
Nominal power factor	0.8922	pu
Nominal efficiency	0.9686	pu
Locked rotor current	3.11	pu
Locked rotor torque	0.42	pu
Locked rotor time at full voltage	31.9	s
Breakdown torque	1.42	pu
Motor inertia	1,180.0	kgm2

Note that this motor with the above characteristics is a typical LIC motor, which according to [2] is capable of driving only a load classified as typical LSD.

This motor is not capable of accelerating a load classified with NSD in a suitable time.

Fig.2 shows the attempt to accelerate the compressor considering 80% of the rated voltage.

It can be observed in Fig.2 that with 80% voltage at the motor terminals, the load curve exceeds the motor torque curve around 60% of its synchronous speed. With 100% voltage the motor can accelerate the load, but the 80% voltage requirement is a major deviation to the project specifications and is not allowed. The direct on-line start produces a voltage drop, usually in the order of 20%.

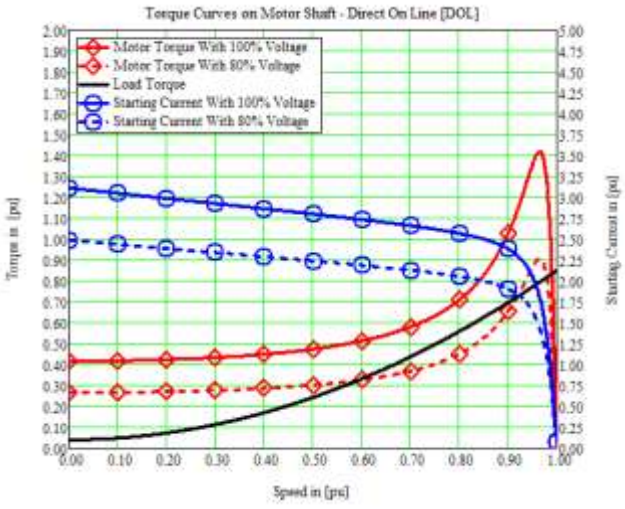

Fig.2 LIC motor and compressor load torque curves.

It can be concluded that a typical LIC motor is not able to drive loads classified as NSD as shown in Fig.1.

Power systems used in the offshore industry are independent, isolated, and supplied by their own generators.

The generators that feed these power systems have an excitation system that recover voltage at the terminals in matter of seconds. This characteristic of generators opens a possibility to resolve the issue of compressor's acceleration, shown in Fig.2 using the typical LIC motor.

Modern AVR applied to generators, provides a high level of automation to the excitation process, which makes them more efficient and reliable in the voltage recovery process.

In Fig.3 the compressor acceleration using the generator voltage recovery process is illustrated. The motor starts directly on the grid with 80% of the nominal voltage, and near to 50% of the nominal rotation, the voltage at the terminals has recovered to 100%.

The compressor acceleration process illustrated in Fig.3 shows that when the voltage recovers during the motor starting process, the typical LIC motor is able to accelerate the load in a suitable time of 24.8s as shown in figure 4.

It is also observed that if the voltage recovery occurs before the motor reaches 50% of the motor's rated speed, around eight seconds, see time interval B in Fig.4, the motor torque curve is far enough away from the compressor torque curve, making the start robust and reliable.

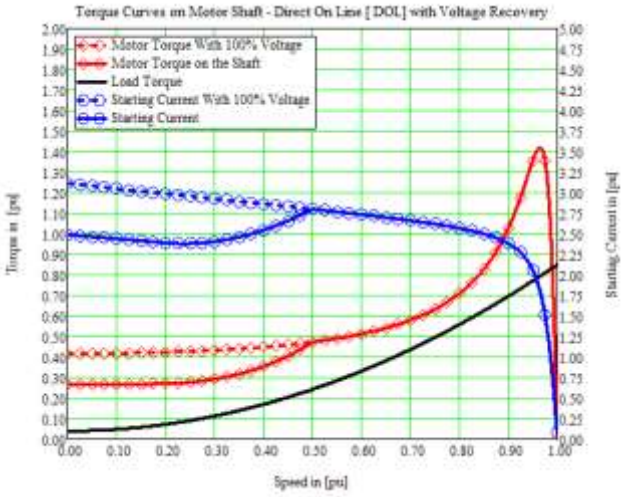

Fig.3 Compressor acceleration with voltage recovery at the LIC motor terminals.

To verify that the voltage recovery starting process is reliable, we also need to perform a transient analysis of the entire process. This analysis must also include the possible voltage drop, during steady state operation. Industry practices normally require that the motor does not stall at a 15% voltage drop, for at least three seconds.

Fig. 4 illustrates the transient compressor start up process with voltage recovery and voltage drop at the end of the simulation.

In Fig. 4, "A" represents the starting time at 80% voltage and voltage recovery.

The time interval "B" represents the time required for voltage recovery by the generator's voltage regulator. Location "C" represents the moment when the nominal load of the compressor is applied to the motor shaft. The interval “D” represents the time range of 4.5s with a 15% voltage drop.

The transient simulation shown in Fig. 4 confirms that the typical LIC induction motor starting with voltage recovery process, also fully meets all specification requirements and is therefore an applicable solution for driving this compressor with a high torque curve that is classified as NSD.

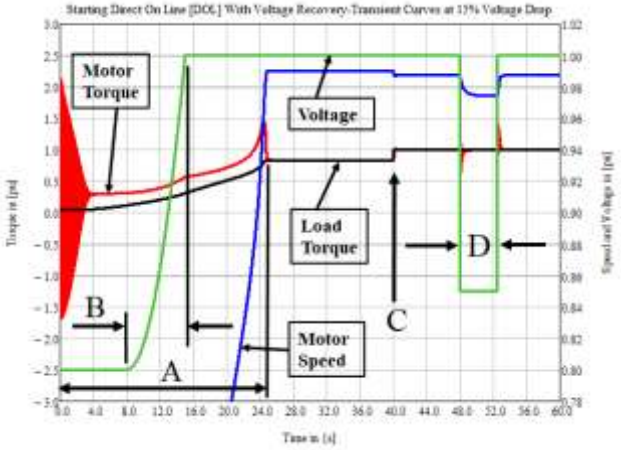

Fig.4 Transient starting process with voltage drop.

It is important to emphasize that the voltage recovery starting method, in addition to ensuring acceleration in a suitable time, maintains impact on the network below the required value of 3.0 pu, according Table III. In Fig. 3 it can be observed that throughout the acceleration process, the starting current remained below 3.0 pu.

III. HIGH TORQUE LOW INRUSH CURRENT MOTOR DESIGN

Another solution to solve the load acceleration issue is to redesign the typical LIC motor squirrel cage to obtain a higher torque. But, according to [2], increasing the breakdown torque also means increasing the motor starting current. Due to the characteristics of the physical behavior of the machine, increasing the breakdown torque to values greater than 1.5 pu also implies to increase the starting current, forcing this current to be greater than 3.0 pu.

Fig. 5 shows the torque curve of the typical LIC motor discussed in sub-chapter II and the torque curve of the typical LIC motor with the redesigned squirrel cage. Note that the new higher torque curve meets the compressor acceleration condition rated NSD even at 80% of rated voltage.

The high-torque LIC motor displays the torque curve at 100% voltage in solid line with circle and accelerates the load in 10.7s. For 80% voltage, however, it shows the torque curve in dotted line with circle and accelerates the load in 24.9s.

The improvement of the torque curve for the high torque LIC motor will be discussed in this subchapter III.

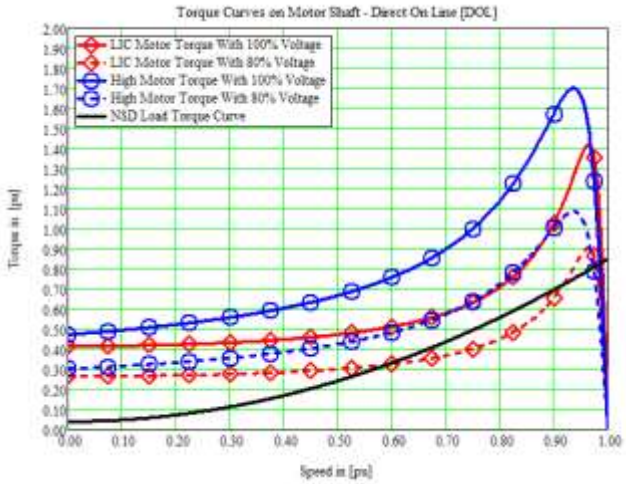

Fig.5 Motor torque curves with redesigned squirrel cage

Fig.6 shows the current curves of the typical LIC motor discussed in sub-chapter II and the current curves of the redesigned LIC motor.

As previously stated, when the LIC motor’s design is changed to increase the breakdown torque, the inrush current also increases. The increment in the starting current went from 3.11 pu to 3.29 pu. This current value can still be considered a low starting current, thus maintaining the characteristic of a LIC motor, but with a higher torque.

In order to obtain an electromagnetic torque curve generated by the motor that can accelerate the load, as shown in Fig 5, but keeping the characteristics of a LIC motor, it is necessary to increase the breakdown torque and decrease the speed at the point of breakdown torque.

With this objective in mind, the stator design data for the two machines, typical LIC motor and high torque LIC motor, will be assumed to be the same. The redesign will be accomplished for the squirrel cage machine rotor, only.

The primary stator design data for the two machines are shown in Table IV.

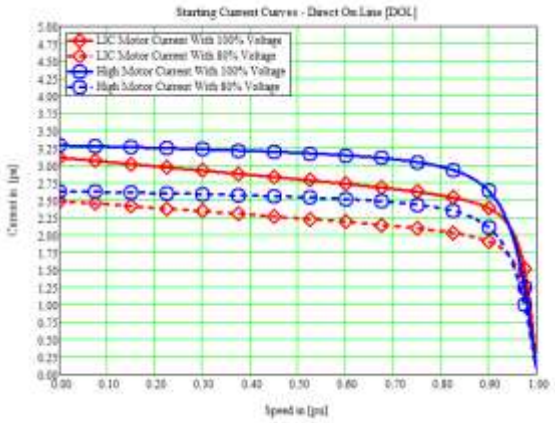

Fig.6 Motor starting current curves with redesigned squirrel cage.

TABLE IV
STATOR DESIGN DATA FOR THE TWO MACHINES

Item	Value	unit
IEC frame	1000	
External diameter	1,800.0	mm
Internal diameter	1,060.0	mm
Core iron length	1,295.0	mm
Air gap	5.0	mm

The slotted stator geometry, with dimensions and distribution of the stator coil conductors is shown in Fig.7(a). The cage bar geometry for the typical LIC motor is shown in Fig 7(b) and the cage bar geometry for the high torque LIC motor is shown in Fig 7(c).

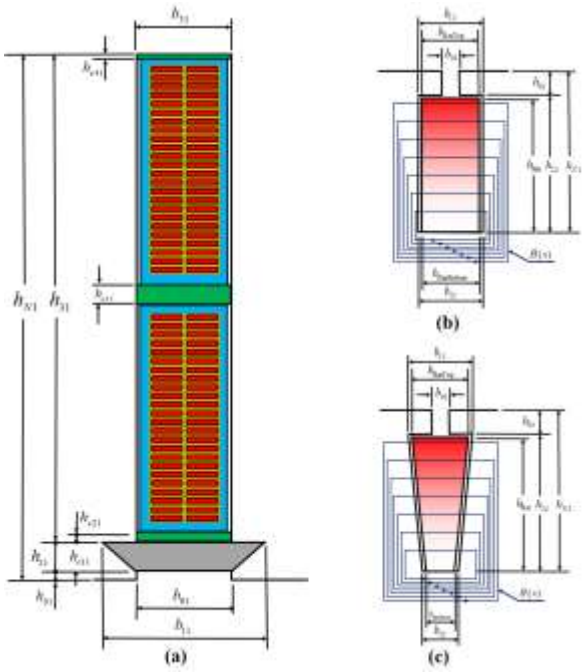

Fig. 7 Stator and rotor slots dimensions – a) Stator - b) Typical LIC motor - c) High Torque LIC motor.

Table V shows the primary characteristics of the typical LIC motor squirrel cage, and the high torque LIC motor squirrel cage.

Note in Table V that the squirrel cage, short circuit ring for the two machines, has the same geometry, and the same dimensions. Only the material has changed resulting in a different electrical conductivity.

The short circuit ring material of the typical LIC motor is die copper with electric conductivity of 80% International Annealed Copper Standard (IACS) and the short circuit ring material of the high torque LIC motor is brass 6436 with electrical conductivity of 25% IACS.

The typical LIC motor squirrel cage bar is rectangular and is a copper alloy with 64% copper and 36% zinc, commonly called 6436 brass with an electrical conductivity of 25% IACS.

The high torque LIC motor squirrel cage bar has been redesigned with trapezoidal geometry and 5832 brass with an electrical conductivity of 20 % IACS.

TABLE V
CHARACTERISTIC OF ROTOR SQUIRREL CAGE

Rotor Characteristics	Typical LIC Motor	High Torque LIC Motor
Rotor slot number	Same	Same
Bar material	Brass 6436	Brass 5832
SC ring material	Die copper	Brass 6436
Bar width at top	17.0 mm	22.0 mm
Bar width at bottom	17.0 mm	18.0 mm
Bar height	55.0 mm	40.0 mm
Skin effect on rotor bar resistance	3.13	1.84
Skin effect on rotor slot reactance	0.47	0.77
Skin effect on the SC ring resistance	10.82	6.3
SC ring external diameter	Same	Same
SC ring internal diameter	Same	Same
SC ring width	Same	Same

The skin effect factor shown in Table V represents the relationship between AC resistance and DC resistance calculated for the rated frequency.

For further details about conductive physical materials, used for this paper, and the squirrel cage motor complex equivalent circuit, refer to the Appendix A.

The squirrel cage leakage reactance for the high-torque LIC motor has decreased by 40.21% compared to the typical LIC motor leakage reactance.

Solving the equivalent circuit shown in the Appendix A (Fig A-I), from zero to synchronous speed for the typical LIC motor and for the high torque LIC motor, will compare the performance of the two motors.

The torque curves of the two motors as a function of rotation for 100% and 80% of the voltage, at the motors' terminals, are shown in Fig 5. Analyzing the torque curves, it can be observed that the typical LIC motor cannot accelerate the load with 80% of the nominal voltage. However, the LIC motor designed for high torque accelerates the load with 80% of the voltage in 24.9s as shown in Figure 11. The same motor, with 100% voltage at the terminals, accelerates the load in a time of 10.7s.

The starting current curves for the two motors, with 100% and 80% voltages at terminals, are shown in Fig 6. For the high torque LIC motor the starting current for 100% voltage is less than 3.3 pu, verifying that the motor still has the characteristics of a LIC motor. Maintaining the characteristics of an LIC motor is the primary design goal of the high-torque LIC motor, that is why the redesign of the LIC motor was focused to increase the torque but keeping a starting current around 3.0 pu.

Table VI shows other performance characteristics of the two motors.

In Table VI, further right column, the changes of the performance characteristics are shown. The performance quantities of the typical LIC motor were considered as base values.

TABLE VI
MOTOR MAIN PERFORMANCE DATA

Performance Characteristics	Typical LIC Motor	High Torque LIC Motor	Variation (%)
Starting current [pu]	3.11	3.29	5.788
Locked Rotor torque [pu]	0.42	0.47	11.190
Breakdown torque [pu]	1.42	1.71	20.423
Speed at breakdown torque [pu]	0.96453	0.93673	-2.882
Slip at breakdown torque (%)	3.5469	6.3268	78.375
Locked rotor time [s]	31.9	25.0	-21.630
Efficiency [pu]	**0.9686**	**0.9633**	**-0.5481**
Power factor [pu]	**0.8922**	**0.9209**	**3.221**
Nominal current in [A]	847.82	829.13	-2.2046
Stator stray losses [kW]	42,755.15	43,954.04	2.8041
Stator Joules losses [kW]	98,981.52	93,951.67	-5.0816
Stator iron losses [kW]	47,391.87	55,097.87	16.260
Rotor stray losses [kW]	48,693.50	45,939.20	-5.6564
Rotor iron losses [kW]	0.605981	0.989836	63.344
Rotor bar losses [kW]	**168,165.3**	**228,502.07**	**35.879**
SC Ring losses [kW]	**30,321.00**	**72,496.07**	**139.09**
Total rotor losses [kW]	198,486.3	300,998.14	51.647
Mechanical losses [kW]	146,255.6	144,669.48	-1.0845
Total losses [kW]	583,169.9	685,600.24	17.564

The increase in load acceleration capacity NSD shown in Figure 5 was obtained at the expense of increasing the resistance and decreasing the leakage reactance of the squirrel cage design. Therefore, it was necessary to increase the resistivity of the material of the bars and the short circuit ring and, associated with this change, the geometry of the rotor slot was changed from rectangular to trapezoidal.

These changes produced a very significant increase in slip at the point of breakdown torque by shifting the motor torque curve to the left and together, with the increment of the breakdown torque, greatly increased load acceleration capacity. The slip at the point of breakdown torque is shown in Table VI and corresponds to an increase of 78,375%.

These changes affected positively the motor's power factor and negatively its efficiency. The motor's efficiency and power factor are highlighted in Table VI. The decrease in efficiency is a direct consequence of the increment on joule losses, generated by the squirrel cage due to the need of shifting the motor torque curve, further to the left and thus increasing its slip.

The most intense effect of the squirrel cage redesign was the thermal effect. There was a significant increment of joule losses in the bar and in the short circuit ring. At the bar, there was an increase in the order of 36% of losses. In the ring, the increment of joule losses, was more in the order of 140%, because the electrical resistivity of the material increased it significantly.

This increment of joule losses in the squirrel cage implied an overall increment of machine losses of the order of 17.56%. These increased losses have a negative impact on machine efficiency. Joule losses in the squirrel cage are highlighted in Table VI.

Losses on the stator side were practically the same for the two machines because no design changes were made to the high torque LIC motor's stator.

It should be noted that the increase in total motor losses of 17.56% implies a consumption of approximately 100.0 kW more, by the high torque LIC motor, representing approximately 0.56% losses of the rated power of the machine. This increase in energy consumption during the entire life of the motor increases the burning of gas and consequently increases emissions.

This increment, of squirrel cage joule losses, produces an increase in the heating of the bars and short circuit ring. The additional heating due to increased losses needs to be analyzed both at the load starting process, and at steady state of motor operation.

Fig.8 shows temperature variation in (K/s) of the squirrel cage bar and short circuit ring for 100% of the voltage applied to the motor during the starting process, as a function of machine's acceleration time.

Note that the heating of the different parts of the cage takes place in a different way. The top of the bar is subject to greater heating due to the electric current displacement, reaching a temperature rise of around 100 K, at the end of the starting process.

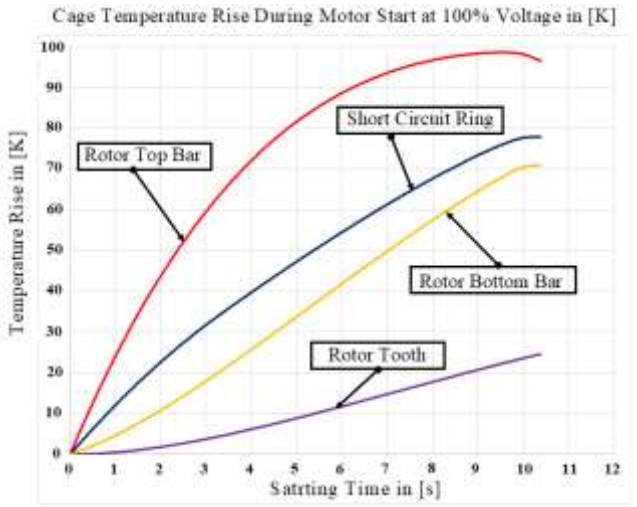

Fig. 8 Squirrel cage temperature in [K] during starting process with 100% Voltage.

The lower part of the bar is subject to much less heat because the current density at the bottom is lower than at the top. The temperature difference between the upper and lower part of the bar introduces thermal stress that must be properly analyzed, so it does not exceed the limit of the mechanical strength of the bar material [4].

The heating of the short circuit ring behaves in a more linear fashion than the top of the bar because the thermal dissipation to the air during the starting process is poorer, making it approach an adiabatic system.

In the final moments of the starting process, the temperature at the top of the bar decreases some, since the skin effect is much smaller during these moments.

Fig. 9 shows the temperature variation in (K) at the bar and at the short circuit ring, for 80% of voltage applied to the machine terminals, during the load acceleration process.

Fig. 9 shows the heating as well in (K) of the bar and short-circuit ring during the process of two consecutive starts, for 80% of the nominal voltage applied to the machine terminals.

The temperature rise of the bar and the short circuit ring at the end of the first start is much higher than the temperature rise when the motor starts at 100% voltage, refer to Fig. 8.

The temperature difference between the top and the bottom of the bar is smaller because the acceleration time is longer so the heat generated at the top can propagate to the bottom.

This smaller temperature difference is desirable because it lowers the thermal stress at the top of the bar.

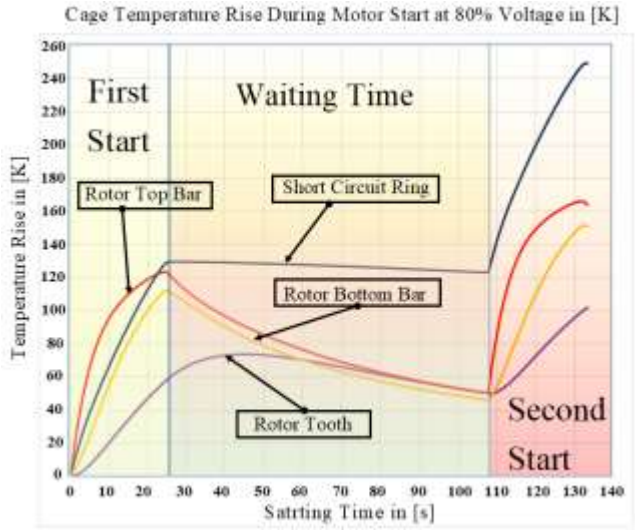

Fig.9 Squirrel cage temperature rise during starting process with 80% voltage.

Fig 9 shows the heating of the short circuit ring at the end of the first start, which is greater than the heating of the top of the bar. This fact is associated with large losses generated in the ring due to the skin effect and due to the poor thermal dissipation of the cooling air during the start-up process.

The greater heating is a consequence of the longer acceleration time during the starting process with 80% of the voltage, which is in the order of 24.9s as shown in Fig. 11.

In the time interval between the two starts, the bar cools down with greater intensity. Cooling takes place due to the heat generated in the bar is transferred to the steel in the plate tooth. After certain time the temperature of the plate tooth approaches to the temperature of the top of the bar.

In the same time interval between the two starts, the temperature of the short circuit ring did not decrease significantly. Due to the difficulty of the short circuit ring transferring heat to the air, it becomes a critical cage component in terms of the number of motors starts.

From the analysis of the heating of the bar and the short circuit ring shown in Fig.8 and Fig.9 it can be concluded that the temperature of the bar and the short circuit ring at the end of the load acceleration stabilizes at a higher value. These high temperature values for both the bar and the ring are a consequence of the increment of losses introduced in the starting process. This increment of losses occurs because, in the redesign of the squirrel cage, it was required to increase the resistance of the cage, to achieve the defined goal, which was to increase the motor's electromagnetic torque curve.

The amount of heat generated during the load acceleration process depends on the joule's losses in watts, and the acceleration time in seconds. The acceleration time for 100% voltage is 10.7s and the load acceleration time for 80% voltage is 24.9s. As the acceleration time with 80% of the voltage is greater, the heat generated in this condition in the acceleration process is greater, implying that the temperature of both the bar and the short circuit ring, at the end of the acceleration is much higher, as shown in the graphs of Fig.9.

The high temperature variation in the starting process needs to be analyzed in depth. Some precautions must be considered to keep mechanical stress and thermal expansion effects under control.

The first concern is related to the squirrel cage cooling system operating in steady state, it must be ensured that the absolute temperature of the cage is less than 200 degrees Celsius. Considering the ambient temperature of 40 degrees Celsius, the temperature rise of the cage must be maximum of 160 K.

In steady state, the temperature of the short circuit ring must be looked at closely. As the ring is in the air, heat transfer is a little worse than in the bars that are in contact with the rotor iron. However, it is possible to introduce some design feature to ensure greater dissipation of the additional generated heat, and thus keep the operating temperature below the maximum allowable value.

It is not the objective of this paper to discuss the improvements that should be made to the rotor design; however, the motor's manufacturer knows what improvements need to be implemented.

The second concern is related to the heating during the load acceleration process.

Fig. 9 shows the greatest heating in the bar and in the short circuit ring when the machine starts with 80% voltage at the terminals. This heating limits the number of starts the motor can perform.

Considering that the assumed temperature limit of the squirrel cage components, that this motor designed with this squirrel cage can perform in safe condition, is two consecutive starts at ambient temperature and a maximum of one hot start.

If for some reason it is necessary to make two hot starts, it is necessary to wait a time interval of at least 0.5hrs before executing the second start. This restriction must be observed to ensure the physical integrity of the squirrel cage, and thus not affect the expected machine's lifetime.

For high peripheral speed machines, mainly II and IV pole, high mechanical strength non-magnetic retaining ring must support the short circuit rings.

Fig 10 shows a squirrel cage rotor with non-magnetic retaining ring.

Fig.10 Squirrel cage rotor with non-magnetic retaining ring.

When the retaining ring is needed, it is necessary to carry out a detailed analysis of the stresses arising from the thermal expansion of the short circuit ring produced by the heating in the starting process. In this analysis, it is also required to consider the effects arising from the acceleration of the load from, zero up to nominal speed.

In the bar of the squirrel cage, the heating along the height, due to the current displacement effect, is subject to uneven heating. The cage bar being designed with a conductive material of lower conductivity, has less current displacement effect causing the bar heating not to be so uneven in height.

Even though this effect is less pronounced, an analysis of the thermal effect between the upper and lower part of the bar is necessary to ensure that the cage performs well [4]. The effect caused by uneven heating between the top and the bottom of the bar bends the bar and introduce tensile stresses at the top of the bar.

Designing the squirrel cage of a high-torque LIC motor that can accelerate an industrial load rated NSD is not an easy task, but clearly not an impossible one. Considering that today Engineering has virtual simulation resources of high efficiency and accuracy, it is possible to carry out the necessary studies and analysis to ensure the reliable performance of the motor.

Once the squirrel cage has been redesigned to generate the required torque curve, while maintaining the characteristics of an LIC motor, it is finally required to carry out a complete transient analysis of the entire load drive process. This analysis also needs to include the possible voltage drops in steady state operation.

Fig.11 illustrates the transient compressor start up process by high torque LIC motor, with voltage drop at the end of the simulation.

In Fig.11, “A” represents the starting time at 80% voltage. The instant of time B represents the moment when the nominal voltage is applied to the motor terminals. Instant "C" represents the moment when the nominal load of the compressor is applied to the motor shaft. The interval “D” represents the time range of 4.5s with a 15% voltage drop.

The transient simulation shown in Fig.11 confirms that the high torque LIC induction motor starting with 80% voltage, also fully meets all specification requirements and is therefore an applicable solution for driving this compressor with a high torque curve, that is classified as NSD.

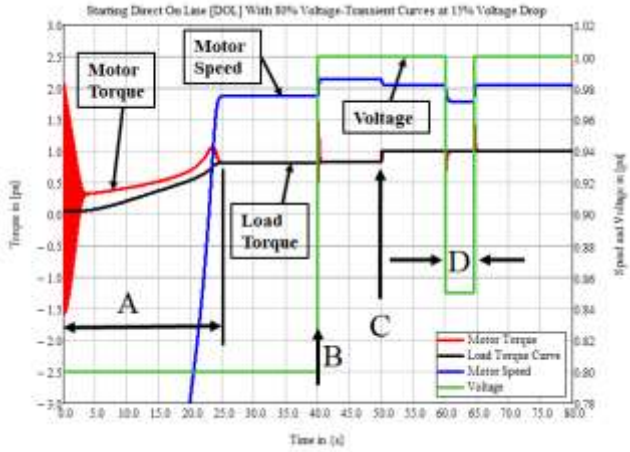

Fig.11 Transient starting process with voltage drop.

IV. CONCLUSIONS

A comparative analysis of the two solutions analyzed in this paper, for the drive of industrial load classified as NSD, that is, for loaded start condition, allows us to state:

1. The solution with the typical LIC motor using the voltage recovery method is feasible as long as voltage recovery system is available, reliable, and fast enough to ensure that during load acceleration the nominal voltage is restored. This solution imposes less thermal stress on the motor during the starting process.
2. The solution with the high torque LIC motor presents itself as a more robust solution, as it does not depend on the voltage recovery system. This solution imposes greater thermal stress on the motor in the load acceleration process. As a result, the motor is more sensitive to the number of starts.
3. Even with this limitation of number of starts the high torque LIC motor is still a very attractive alternative when compare to:
   - Having to invest in the generation system that can sustain DOL motors’ inrushes of these large motors, or
   - Having to invest in soft-starting methods (i.e.: ASD, soft starters, etc) to be able to start these large motors, in facilities where topsides space is a luxury.

   For either one of the listed above, the cost associated with such solutions, for offshore facilities, is estimated to be significantly much higher than the implementation of high torque LIC motor.
4. It is possible to design a LIC motor with high torque to accelerate a load rated NSD while keeping low the impact on the power supply or consumption.

5. Although minimum, the efficiency reduction for the high-torque LIC motor implies in an increment on gas consumption, to compensate the increase on losses.
6. The design of the high-torque LIC motor requires a greater effort, in both correctly choosing the conductive material to be used, and the analysis that must be carried out to ensure the thermal and mechanical performance of the squirrel cage.
7. When the load classified as NSD has starting torque closer to the upper limit 0.50 pu, the higher torque LIC motor design becomes more complex, but it is possible to keep the starting current within the accepted limit for LIC motor approaching 4.0 pu.
8. In systems with their own power generation, voltage recovery during the direct starting process on the grid is always available. However, this feature is not always used in the starting condition of loads classified as NSD. This paper has shown that two solutions are viable, the typical LIC motor with voltage recovery or the use of the high torque LIC motor. The decision of which solution to adopt is up to the customer after a detailed analysis of the application.

V. REFERENCES

[1] Rüncos, Fredemar, Design Fundamentals and Performance analysis of Three-Phase Electrical Machines, second edition, Volumes 4, 1675p, Publisher 893, Jaraguá do Sul - SC-Brazil.

[2] Rüncos, Fredemar, Benefits-And-Drawbacks-Of-Low-Inrush-Large-Induction-Squirrel-Cage-Electric - Motors, PCIC 2018.

[3] Janssen, Wilfried, “Praxisnahe Berechnung der Anzugs und Hochlufdaten schnellaufender käfigläufer”, Hannover University.

[4] Bredthauer, Jürgen and Struck, Norbert “Starting of Large Medium Voltage Motors: Design, Protection, and Safety Aspects”, IEEE Transactions on Industry Applications, Vol. 31, NO. 5, September/October 1995.

[5] Kirtley, L. James “Designing Squirrel Cage Rotor Slots with High Conductivity”, Massachusetts Institute of Technology, Massachusetts, 02139, USA.

[6] Madu Thirugnanasambandamoorthy, P.Eng, Christophe del Perugia, Bharat Mistry, P.Eng ,”What does it take to design a low inrush large induction motor?”, PCIC-2011-13..

VI. NOMENCLATURE

AVR	Alternator Voltage Regulator.
ASD	Adjustable speed drive.
DOL	Direct on line.
FPU	Floating Production Unit.
HSD	Heavy Starting Duty.
LIC	Low Inrush Current.
LSD	Light Start Duty.
NSD	Normal Start Duty.

VII. VITAE

Fredemar Rüncos received the Engineering and Physics degrees from the Federal University of Paraná, Brazil in 1980. In 2002 and 2006 he received his M.Sc. and Ph.D. degrees in electrical engineering, respectively, from the Federal University of Santa Catarina, Brazil. In 1990 he became the manager of the product engineering department of WEG Energy for large rotating electrical machines. In 2009 He became manager of the D&TI department of WEG Energy. At present, he is a D&TI consultant and Professor in the electrical engineering department of the Catholic University Center of Santa Catarina. His research interests surround induction and synchronous machines, including developing methods to analyze the performance and vibration, design criteria and control of a Brushless double fed induction machine with rotary transformer and permanent magnet synchronous machines.

Michael Bachmeyer is presently Vice President for North America, WEG Global Oil & Gas Group. In addition to experience in all industrial electrical equipment, he has 43 years directly in MV/HV rotating electrical machines; 30 years with Westinghouse and now 13 with WEG. All 43 of these years has been Oil & Gas concentrated. Michael is an IEEE member and a past committee member of the API group that penned the API motor specifications.

Miguel Sarris graduated from the Central University of Venezuela, Venezuela in January of 2000 with a BSEE degree (in Power systems). He is presently the Electrical Engineering Team Lead for Doris Inc, the US affiliate for Doris Group. His experience from the Operator and Customer side, to the Engineering Consulting service provider designing, specifying, testing, and commissioning HV & LV electrical equipment sum over 22 years; all these years have been Oil & Gas focused, with global experience based on projects located from Latin and Central America, Caribbean, US, to Europe and Africa. He is a Professional Engineer registered under the boards of: State of Texas – USA, Australia, and Venezuela.

Adrain Stafford received an Electrical Engineering degree from the University of Houston in 2007. She interned at American Bureau of Shipping (ABS) and is presently an Electrical Engineer for MODEC International Inc. since 2007. She has 14 years of experience in industrial electrical equipment used for offshore oil and gas platforms, primarily Floating Production Storage and Offloading Vessels.

APPENDIX A

Table A-I shows the physical properties of some conductive materials that were explored during the design process of two potential squirrel cages for the LIC motor.

TABLE A-I
CONDUCTIVE MATERIALS - PHYSICAL PROPERTIES

Material	$\gamma \cdot 10^3$ (kg/m3)	$\sigma \cdot 10^6$ (S/m)	$\alpha \cdot 10^{-4}$ (1/K)	c (J/kgK)	λ (W/mK)
Copper	8.90	58	39.29	394.0	372
Die Copper	8.90	46.4	39.29	394.0	372
Brass 9505	8.85	32.3	21.90	385.0	234
Brass 8515	8.75	21.5	14.60	380.0	178
Brass 6436	8.47	15.0	10.20	377.0	126
Brass 5832	8.30	11.6	7.422	377.0	95
C63000	7.5	5.22	3.45	376.8	37.7

The term γ represents the density, σ the conductivity, α the temperature coefficient and c the specific heat and λ the thermal conductivity of the conductors material.

Once the squirrel cage of the high torque LIC motor has been redesigned, a detailed load performance analysis must be performed. o make this detailed analysis we will consider the equivalent circuit of the asynchronous machine shown in Fig A-I.

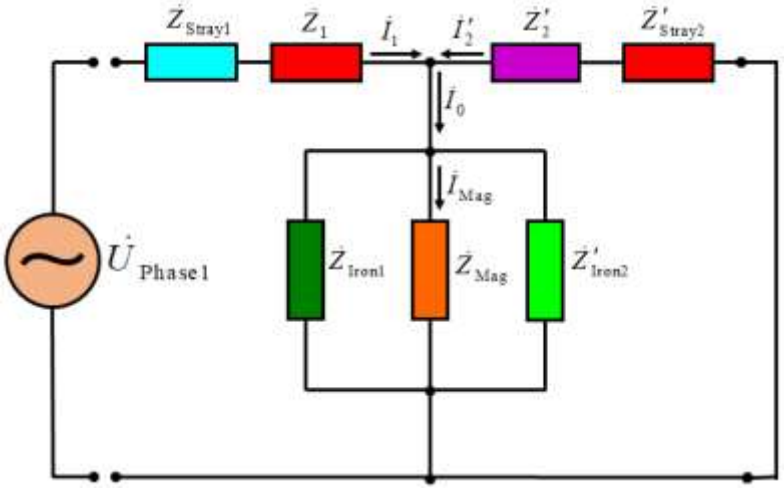

Fig. A-1 Squirrel cage motor complex equivalent circuit

The following relations give the complex impedances shown in the equivalent circuit in Fig 9:

The stator phase supply voltage:

$$\dot{U}_{\text{Phase1}} = U_{\text{Phase1}} + j \cdot 0 \tag{4}$$

The stator phase stray losses impedance:

$$\dot{Z}_{\text{Stray1}} = R_{\text{Stray1}} + j \cdot 0.00 \tag{5}$$

The stator phase impedance:

$$Z_1 = R_1 + j \cdot X_1 \tag{6}$$

The rotor phase impedance:

$$Z'_2 = \frac{R'_2}{s} + j \cdot X'_2 \tag{7}$$

The rotor phase stray losses impedance:

$$\dot{Z}'_{\text{Stray2}} = \frac{R'_{\text{Stray2}}}{s} + j \cdot 0.00 \tag{8}$$

The stator phase iron losses impedance:

$$\dot{Z}_{\text{Iron1}} = R_{\text{Iron1}} + j \cdot 0.00 \tag{9}$$

The rotor phase iron impedance:

$$Z'_{\text{Iron2}} = \frac{R'_{\text{Iron2}}}{|s|} + j \cdot 0.00 \tag{10}$$

All rotor parameters are referred to the stator.

The magnetizing impedance:

$$Z_{\text{Mag}} = 0.00 + j \cdot X_{\text{Mag}} \tag{11}$$

The slip s of the motor in per unit is defined as:

$$s = \frac{f_{\text{e1}} - p \cdot f_{\text{Mec}}}{f_{\text{e1}}} \tag{12}$$

Where:

$R_1 \Rightarrow$ Stator phase resistance.

$X_1 \Rightarrow$ Stator phase leakage reactance.

$R_{\text{Stray1}} \Rightarrow$ Stator phase equivalent stray losses resistance.

$R'_2 \Rightarrow$ Rotor phase resistance.

$X'_2 \Rightarrow$ Rotor phase leakage reactance.

$R'_{\text{Stray2}} \Rightarrow$ Rotor phase equivalent stray losses resistance.

$s \Rightarrow$ Represents the slip of the motor.

$R_{\text{Iron1}} \Rightarrow$ Stator phase equivalent iron losses resistance.

$R'_{\text{Iron2}} \Rightarrow$ Rotor phase equivalent iron resistance.

$X_{\text{Mag}} \Rightarrow$ Motor magnetizing reactance.

In equation (12) f_{e1} represents the supply voltage frequency given in Hz, f_{Mec} represents the rotor mechanical speed given in Hz and p is the number of pole pairs. Table A-II shows the quantities of complex impedances for the typical LIC motor and for the high-torque LIC motor. All resistances are referenced to 95ºC.

TABLE A-II

EQUIVALENT CIRCUIT IN COMPLEX FORM DATA

Impedances at 95.0 ºC	Typical LIC Motor	High Torque LIC Motor
$\dot{U}_{\text{Phase1}} = U_{\text{Phase1}} + j \cdot 0.0$	$\frac{13{,}800.0}{\sqrt{3}} + j \cdot 0.0$	$\frac{13{,}800.0}{\sqrt{3}} + j \cdot 0.0$
$\dot{Z}_{\text{Stray1}} = R_{\text{Stray1}} + j \cdot X_{\text{Stray1}}$	$(19.066 + j \cdot 0.00) \cdot 10^{-3}$	$(20.650 + j \cdot 0.00) \cdot 10^{-3}$
$\dot{Z}_1 = R_1 + j \cdot X_1$	$(42.204 + j \cdot 2{,}019.828) \cdot 10^{-3}$	$(42.204 + j \cdot 2{,}019.828) \cdot 10^{-3}$
$Z'_2 = \frac{R'_2}{s} + j \cdot X'_2$	$\left(\frac{83.018}{s} + j \cdot 1{,}580.097\right) \cdot 10^{-3}$	$\left(\frac{135.258}{s} + j \cdot 944.715\right) \cdot 10^{-3}$
$Z'_{\text{Stary2}} = \frac{R'_{\text{Stary2}}}{s} + j \cdot X'_{\text{Stray2}}$	$\left(\frac{22.575}{s} + j \cdot 0.00\right) \cdot 10^{-3}$	$\left(\frac{22.275}{s} + j \cdot 0.00\right) \cdot 10^{-3}$
$Z_{\text{Iron1}} = R_{\text{Iron1}} + j \cdot X_{\text{Iron1}}$	$(3{,}366.74 + j \cdot 0.00)$	$(2{,}995.13 + j \cdot 0.00)$
$Z'_{\text{Iron2}} = \frac{R'_{\text{Iron2}}}{\lvert s \rvert} + j \cdot X'_{\text{Iron2}}$	$\left(\frac{3{,}566.740}{\lvert s \rvert} + j \cdot 0.00\right)$	$\left(\frac{3{,}152.542}{\lvert s \rvert} + j \cdot 0.00\right)$
$Z_{\text{Mag}} = R_{\text{Mag}} + j \cdot X_{\text{Mag}}$	$(0.00 + j \cdot 109.250)$	$(0.00 + j \cdot 102.095)$
$s = \frac{f_{\text{e1}} - p \cdot f_{\text{Mec}}}{f_{\text{e1}}}$	$\left(\frac{60 - 2 \cdot f_{\text{Mec}}}{60}\right)$	$\left(\frac{60 - 2 \cdot f_{\text{Mec}}}{60}\right)$

Note in Table A-II that the squirrel cage redesign of the high-torque LIC motor increased the rotor resistance by 62.93% over the rotor resistance of the typical LIC motor.